Bioinspired Approach to Modeling Retinal Ganglion Cells Using System Identification Techniques

Philip J. Vance, Gautham P. Das, Dermot Kerr, Sonya A. Coleman, T. Martin McGinnity, *Senior Member, IEEE*, Tim Gollisch, and Jian K. Liu

***Abstract*— The processing capabilities of biological vision systems are still vastly superior to artificial vision, even though this has been an active area of research for over half a century. Current artificial vision techniques integrate many insights from biology yet they remain far-off the capabilities of animals and humans in terms of speed, power, and performance. A key aspect to modeling the human visual system is the ability to accurately model the behavior and computation within the retina. In particular, we focus on modeling the retinal ganglion cells (RGCs) as they convey the accumulated data of real world images as action potentials onto the visual cortex via the optic nerve. Computational models that approximate the processing that occurs within RGCs can be derived by quantitatively fitting the sets of physiological data using an input–output analysis where the input is a known stimulus and the output is neuronal recordings. Currently, these input–output responses are modeled using computational combinations of linear and nonlinear models that are generally complex and lack any relevance to the underlying biophysics. In this paper, we illustrate how system identification techniques, which take inspiration from biological systems, can accurately model retinal ganglion cell behavior, and are a viable alternative to traditional linear–nonlinear approaches.**

***Index Terms*— Artificial stimuli, biological vision, computational modeling, receptive field (RF), retinal ganglion cells (RGCs).**

I. Introduction

MIMICKING biological vision systems have been a consistent challenge in the artificial vision research field for many years. Vision begins with light that is projected to the back of the eye onto the retina, which is an extension of the brain approximately 0.3–0.4 mm thick and covers an area of approximately 520 mm^2 [1]. Around 125 million rods and cones, photoreceptors transform visible light into neural signals [2]. This is in comparison to 1 million ganglion cells, which receive the signal information, having been filtered through intermediate layers consisting of horizontal, bipolar, and amacrine cells. There are around 15–20 distinct types of retinal ganglion cells (RGCs), which transform the signal information into what are known as action potentials (spikes) and transmit the information via synaptic connections to the visual cortex for higher processing. Previously, the retina was thought of as a simple spatiotemporal filter, with the real processing beginning in the visual cortex. However, this view has been substantially revised in recent times [4].

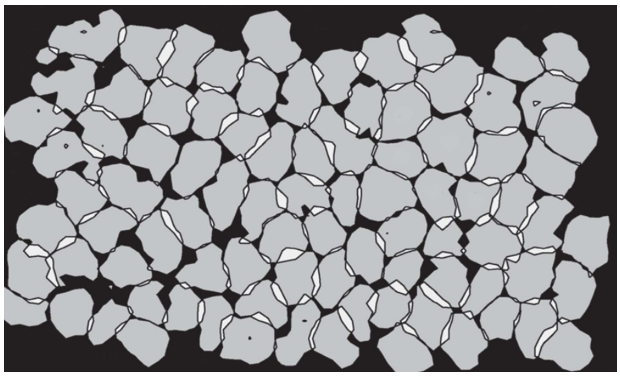

Fig. 1. Recorded RFs from "parasol" ganglion cells in macaque retina. (Figure adapted from [3] according to the Creative Commons Attribution License.)

There is very little feedback from the brain to the retina; thus, it is an ideal biological system to derive the computational models of a stimulus–response relationship, as the inputs can be precisely controlled whilst the output can be extracellularly recorded from RGCs through the use of a multielectrode array [5]. Each RGC pools signals from multiple photoreceptors via a networked infrastructure of the various cell types. Collectively, the spatial area of photoreceptors, which contribute to an RGC, eliciting a response is known as the receptive field (RF), which can also be referred to as the region of the sensory space in which visual stimulus triggers a neuron to fire. The general shape of this spatial area is commonly approximated to be either a circular [6] or an elliptical region that is often defined with a 2-D Gaussian spatial profile [7], [8]. In reality, however, the actual shape of the RF is highly irregular as demonstrated in Fig. 1 where RGCs from macaque monkeys are shown to

Manuscript received March 9, 2016; revised November 10, 2016; accepted March 22, 2017. Date of publication April 12, 2017; date of current version April 16, 2018. This work was supported by the European Union Seventh Framework Program (FP7-ICT-2011.9.11) under Grant 600954 through the Project VISUALISE. *(Corresponding Author: Philip J. Vance.)*

P. J. Vance, G. P. Das, D. Kerr, and S. A. Coleman are with the Intelligent Systems Research Centre, Ulster University, Magee Campus, Londonderry BT48 7JL, U.K. (e-mail: p.vance@ulster.ac.uk; g.das@ulster.ac.uk; d.kerr@ulster.ac.uk; sa.coleman@ulster.ac.uk).

T. M. McGinnity is with the Intelligent Systems Research Centre, Ulster University, Magee Campus, Londonderry BT48 7JL, U.K., and is also with the College of Science and Technology, Nottingham Trent University, NG11 8NS Nottingham, U.K. (e-mail: tm.mcginnity@ulster.ac.uk).

T. Gollisch is with the Department of Ophthalmology, University Medical Center Göttingen, 37073 Göttingen, Germany, and also with the Bernstein Center for Computational Neuroscience Göttingen, 37077 Göttingen, Germany (e-mail: tim.gollisch@med.uni-goettingen.de).

J. K. Liu was with the Department of Ophthalmology, University Medical Center Göttingen, Göttingen, Germany, and also with the Bernstein Center for Computational Neuroscience Göttingen, 37073 Göttingen, Germany. He is now with Theoretical Computer Science, Graz University of Technology, A-8010, Graz, Austria (email: jian.liu@med.uni-goettingen.de).

Color versions of one or more of the figures in this paper are available online at http://ieeexplore.ieee.org.

Digital Object Identifier 10.1109/TNNLS.2017.2690139

closely interlock and span the entire area of the visual window. Derived models which accurately describe this relationship progress our functional understanding of the retina and inspire future image processing research [9]. In fact, biologically inspired models of the retina, between stimulus and response, have been shown to outperform various machine vision techniques in terms of speed, power, and performance [10].

Modeling of these temporal neural recordings, however, is challenging due to insufficient knowledge about the internal structure and interconnections between cells. Linear–nonlinear (LN) cascades are a popular class of quantitative models used to describe the stimulus–response relationship [11]. In particular, LN models have been used to describe the processing in the retina [12] though the main drawback is that they lack any relationship between the derived parameters and underlying biophysics of the system [11]. System identification tools are useful in this case as they are suited to dynamical systems and allow for a better insight into the underlying physics of the biological system. First, to understand the responses of auditory neurons [13], output responses were recorded using white noise stimuli and inferences were made on mapping the stimulus to the response. As is often the case, white noise stimulation is preferred for modeling biological vision systems [14] as it remains controlled and is easily analyzed mathematically. However, there is evidence that the use of artificial stimuli produces models that do not adequately describe responses to natural visual scenes [15]. Therefore, models created under these conditions using artificial stimuli may only be considered a subset of the full biological model under certain conditions.

Artificial neural network (ANN) methodologies, by definition, are designed to mimic the biological aspects of the human brain [16] and through extension, the vision system. Specifically, nonlinear autoregressive network with exogenous inputs (NARX) and k-nearest neighbors (kNNs) approaches have been applied to neural encoding models in human vision [17] whilst methods, such as time delayed neural network, multilayer perceptron, and other ANN implementations, have been used to derive the models of retinal ganglion cell visual processing [18]–[20]. The nonlinear autoregressive moving average with exogenous inputs (NARMAX) model [21]; a parametric system identification technique, which is a natural extension to nonlinear autoregressive exogenous (NARX), has also been used within vision studies to model adaptation of photoreceptors to light in flies [22]. The NARMAX technique lends itself to a broad range of applications in several areas which include modeling robot behavior [23], time series analysis [24], iceberg calving and detecting, and tracking time-varying causality for EEG data [25]. In previous work, [19], [26], the NARMAX methodology has been utilized to help formulate a retina modeling development process and in particular, to express the biological input–output relationship using polynomial models.

The work presented in this paper forms an essential component of the VISUALISE FP7 Project, which seeks to better understand the behavior of the biological retina in order to advance artificial vision systems. The motivation behind this paper is to utilize computational models, which have been derived from biological systems to facilitate fast, robust, and efficient machine vision to overcome the existing weaknesses in artificial vision systems. In this project, we have already deployed the models on a silicon retina.

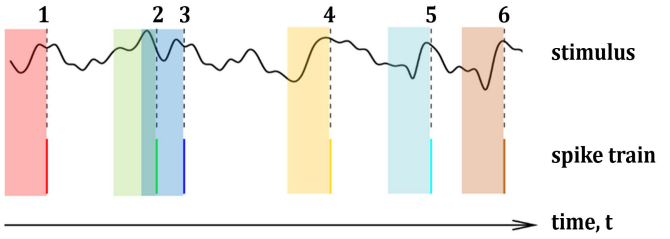

Fig. 2. Calculating spike-triggered average.

In the experiments here, we expand on [26] by introducing, in addition to the NARMAX model, the self-organizing fuzzy neural network (SOFNN) and NARX methodologies. The predictive performance of the investigated methodologies to adequately model a retinal ganglion cell's output is evaluated. Performance is compared amongst these popular approaches, outlined in Section II, with specific reference to the standard LN cascade technique. Section III provides details on the physiological experiments used for data collection and the methods utilized to preprocess the data to form and input–output time series configuration suitable for modeling. The results are presented in Section IV where models have been derived based on two types of artificial stimuli. These models are then analyzed further to determine any underlying system dynamics. Finally, a concluding discussion based on the findings of this paper is presented in Section V along with future directions for investigation.

II. Methods

Deriving a quantitative relationship between stimulus and response of an RGC is challenging if we consider the internal cell structure that precedes them or the numerous interactions over the many interconnections between cells. To simplify this, we consider the problem with a black-box approach, which aims to estimate a mathematical model for a regression data set and apply a number of different methods to form this model. In keeping with traditional approaches, the LN cascade approach is also utilized as a comparison to the investigated approaches.

A. Linear–Nonlinear

The LN cascaded approach is a popular method of estimating the output firing rate of a neuron by applying the input to a linear temporal filter followed by a static nonlinear transformation [11] and can be described by

$$r(t) = F(a * S_t) \tag{1}$$

where a is the temporal linear filter, F is a static nonlinearity, and $a * S_t$ is the convolution of the temporal linear filter and stimulus S_t. The first step in estimating the response of the retina to visual stimuli is to compute the linear filter. This is typically accomplished by computing the spike triggered

average (STA), which is simply the average stimulus preceding each spike (see Fig. 2).

In [14], this is defined by (2), where T is the duration of the stimulus recording and $S_t f_t$ is the stimulus preceding a spike, f_t. Thus, the STA is the sum of all stimuli preceding a spike divided by the total number of spikes within the recording

$$a = \frac{\sum_{t=1}^{T} S_t f_t}{\sum_{t=1}^{T} f_t}. \tag{2}$$

The size of the temporal window is determined by examining the duration of the average response and ascertaining the point at which it converges to zero [14].

Determining the latter element of the LN cascade entails the convolution of the stimulus with the computed STA[$a * S_t$, (1)] and computing the static nonlinearity (F). This is achieved by plotting the spike count as a function of the convolved stimulus and fitting a curve.

B. Nonlinear Autoregressive Exogenous Model

NARX is part of the ANN family and is a model of a nonlinear neural network which accommodates dynamic inputs from a time series type data set. It can learn to predict future values of the time series based on past information from the same time series, feedback input, and an additional time series referred to as the exogenous time series. Based on the same architecture as conventional recurrent neural networks, NARX provide a powerful solution to time series prediction that offers more effective learning and faster convergence over other ANNs [27]. A further advantage in principle is that one can use NARX networks, rather than conventional recurrent networks with complex differentiable nonlinearities, without any computational loss [28].

The topology of the network incorporates input, hidden, and output processing element layers with the input to the network being fed by a number of delay units. Feedback from the output is also fed back to the hidden layer via delay units [29] as shown in Fig. 3.

The description of the example model (Fig. 3) can be denoted as

$$y(t) = f\left(\sum_{i=1}^{N} a_i y(t-i) + \sum_{i=1}^{M} b_i x(t-i)\right) \tag{3}$$

where N, M, a_i, and b_i are constants; $x(t)$ is the source input and $y(t)$ is the output of the network. Previously, NARX have been used to model various elements of the visual system, including human tracking for robot vision applications [30] and the encoding of the natural visual system in humans through *in vivo* experimentation [17]. Although it has been proven that NARX is effective in its predictive performance of complex time series data [31], one of the disadvantages of models created via NARX is that they are not easily analyzed due to their opaque nature in terms of the obtained mapping. This makes it very difficult to understand any underlying system dynamics that might otherwise be apparent in alternative nonlinear system identification methods, for example, NARMAX, which is discussed in Section II.C.

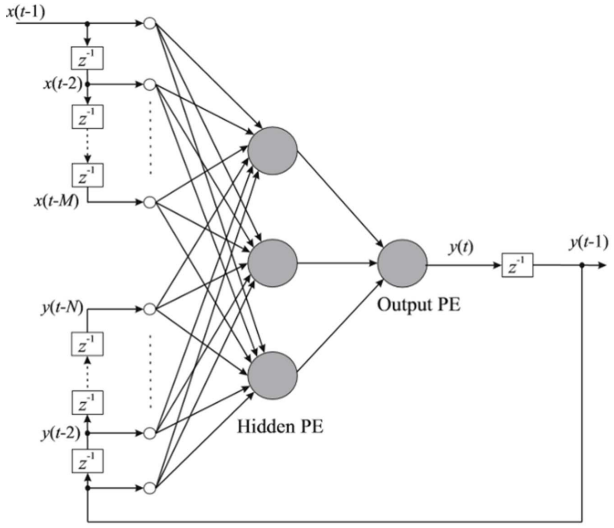

Fig. 3. Architecture of an NARX network [29].

C. Nonlinear Autoregressive Moving Average Model With Exogenous Inputs

A further improvement to the predictive powers of the NARX model can be achieved when the previous errors of the system are integrated as controlled variables [32]. An NARMAX model is formed as the result of this. The NARMAX approach is a popular system identification technique used when attempting to model the nonlinear relationship between the inputs and outputs (stimulus and response). It does this by representing the problem as a set of nonlinear difference equations. The NARMAX model, which is a natural extension of the ARMAX model [33], can be defined by

$$y(t) = F[y(t-1), \ldots, y(t-n_y), u(t-d), \ldots, u(t-n_u), e(t-1), \ldots, e(t-ne)] + e(t) \tag{4}$$

which accounts for the combined effects of noise, modeling errors, and unmeasured disturbances concerning the inputs and outputs. Here, $u(t)$ and $y(t)$ are the input and output vectors, respectively, $e(t)$ is system noise, which is considered bounded and cannot be measured directly, and n_y andn_u are the maximum output and input delays, respectively. $F[.]$, which is an unknown nonlinear function, is typically taken to be a polynomial expansion of the arguments.

To develop an NARMAX model, the structure of the nonlinear equation must first be identified along with the estimation of its parameters. The overall approach is made up of the following steps [25].

1) *Structure Detection:* Determine the terms within the model.
2) *Parameter Estimation:* Tune the coefficients.
3) *Model Validation:* Analyze model to avoid overfitting.
4) *Prediction:* Output of the model at a future point in time.
5) *Analysis:* Analyze model performance and determine the underlying dynamics of the system.

As the structure is typically unknown prior to the implementation, a range of possibilities exist to approximate the function, including polynomial, rational, and various

ANN implementations [33], such as the NARX network. The polynomial models, however, offer the most attractive implementation with regards to visual modeling as they allow for the underlying dynamical properties of the system to be revealed and analyzed. One solution to determine the important terms of the model can be achieved using an orthogonal least squares approach by computing the contribution that each potential model term makes to the system output. Building the system this way, term by term, exposes the significance of each new term added and allows for the avoidance of overfitting due to an excessive use of time lags or nonlinear function approximations [33] by ensuring that the model is as simple as possible and contains good generalization properties. This approach simulates investigative modeling techniques where the important model terms are introduced first and then the model is refined by adding in less significant terms. The only difference is that in the NARMAX method, the model terms can be identified directly from the data set. The unknown parameters and system noise can then be estimated and accommodated within the model. These procedures are now well established and have been used in many modeling domains [34].

D. Self-Organizing Fuzzy Neural Network

Another method which can be utilized to model and analyze time series type data sets is the SOFNN. An SOFNN is a hybrid network, which has the capability to model and forecast a complex nonlinear system. It is capable of self-organizing its architecture by adding and pruning neurons as required based on the complexity of the data set. This alleviates the requirement of predetermining the model structure and estimation of the model parameters as the SOFNN can accomplish this without any in-depth knowledge of neural networks or fuzzy systems. The SOFNN approach has demonstrated good performance in applications of function approximation, complex system identification, and time series prediction, further details of which can be found in [35]–[38].

The main architecture of the SOFNN is a five layer fuzzy neural network as shown in Fig. 4. These include an input layer, ellipsoidal basis function (EBF) layer, normalized layer, weighted layer, and output layer. The SOFNN has the ability to reorganize the connections between these layers during the learning process. In the EBF layer, each neuron is a *T*-norm of Gaussian membership function attributed to the networks inputs (see Fig. 5) where each neuron signifies the if-part of the fuzzy rule. The output from this layer is computed by products of the membership values of each input. The output of the EBF layer is normalized by the third layer, which contains an equal number of neurons, by dividing each output by the sum of all outputs.

The fourth network layer of the network is the weighted layer and signifies the consequent then-part of the fuzzy rules. Each neuron in this layer has two inputs, one of which is directly related to the output of the previous layer whilst the other is fed by a weighted bias. The product of these two inputs translates as the output to the final layer, which contains a single neuron representing the summation of all incoming signals.

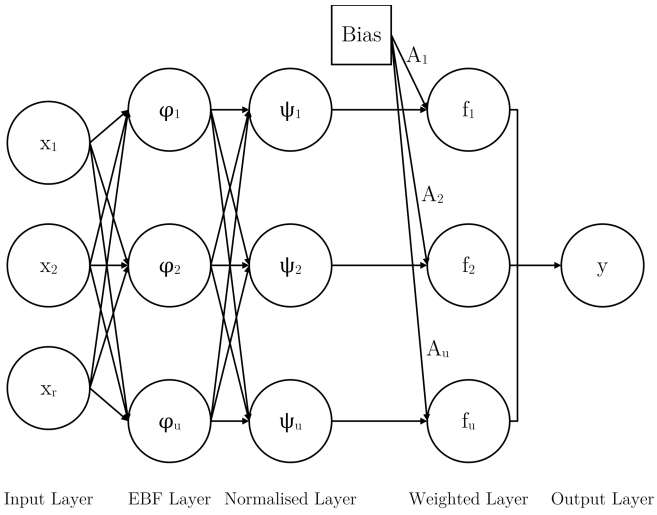

Fig. 4. Layer structure of SOFNN.

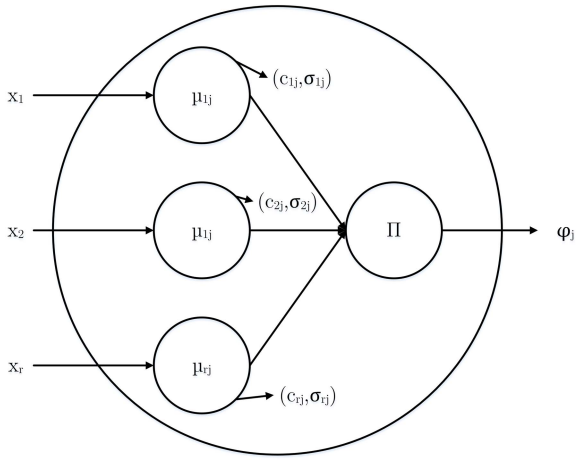

Fig. 5. Internal structure of EBF neuron.

During the learning process of the SOFNN, its internal structure is dynamically modified through adding and pruning of neurons within the EBF layer to achieve an economical network size. Before adding a neuron to the network, existing membership functions are first examined to ascertain whether or not they can be modified to accommodate the new training sample while considering the generalization performance of the overall network. This is determined using the following error criterion:

$$|\epsilon(t)| = |d_t - y_t| \tag{5}$$

where d_t is the desired output of the system and y_t is the network output. If this error is greater than some user-defined threshold δ adding a new EBF neuron to the network will be considered, otherwise an existing membership function may be modified so that it appropriately clusters the new training sample.

Pruning of a neuron is governed by the importance of each neuron based on its contribution to the overall networks performance. The strategy is based on the optimal brain

surgeon approach [39], which uses the second derivative information to find the least important neuron and prune it from the network. If the subsequent performance of the SOFNN remains unchanged, the neuron is permanently deleted. Consequently, the neuron is restored should the performance be significantly degraded. An in depth explanation of the adding and pruning strategy is outlined in [37].

III. Stimulus and Data Preprocessing

Neuronal data were recorded from retinas, which were isolated from dark adapted adult axolotl tiger salamanders, similar to the approach in [5] and [40], where the retina is divided in half, with each half placed cell side down onto a multielectrode array. Each image was projected onto the RGCs by a miniature organic light-emitting diode display with white light. A lens then demagnifies the image and focuses it onto the photoreceptor layer of the isolated retina. The stimulus display ran at 60 Hz whilst the stimulus itself was updated at 30 Hz, meaning a new stimulus presentation was made approximately every 33 1/3 ms. The neural responses (spikes) were recorded at 10 kHz and binned at the stimulus update rate; meaning that all spikes that occur within the stimulus presentation timeframe are summed. Recorded spikes were sorted off-line by a cluster analysis of their shapes, and spike times were measured relative to the beginning of the stimulus presentation.

A. Stimulus

These recordings were performed while under stimulation using temporal and spatiotemporal Gaussian white noise sequences. Artificial white noise sequences are frequently utilized when determining various characteristics of RGCs, including the STA (Section II-A), as this avoids cell adaptation to sustained stimuli, is relatively robust and spans a wide range of visual inputs [14]. An example of the stimulus is shown in Fig. 6, where each image in the temporal sequence Fig. 6(a) and spatiotemporal sequence Fig. 6(b) is presented sequentially. Fig. 6(a) shows a set of uniform intensity temporal images drawn randomly from a normal distributed Gaussian white noise sequence with zero mean and a standard deviation of 1. The sequence is generated using the gasdev() function from the Numerical Recipes library [41]. This sequence is used for full-field illumination, where all pixels within each image are illuminated with the same uniform light intensity; thus, no spatial arrangement is observable. This is referred to as full-field flicker (FFF) and is the least complex form of artificial stimulus used within these experiments. The models derived under these conditions would only be considered a subset of the real neural model as it only considers the temporal component. Thus, Fig. 6(b) extends the stimulus input range to include a spatiotemporal input by introducing the binary checkerboard pattern. The checker-board flicker (CBF) extends the complexity of the input due to an additional spatial component varying randomly across time. In terms of modeling, it allows the incorporation of local spatial summation of information within the complete RF, whereas FFF does not. Each binary checker has a resolution of 10×10 pixels onscreen and

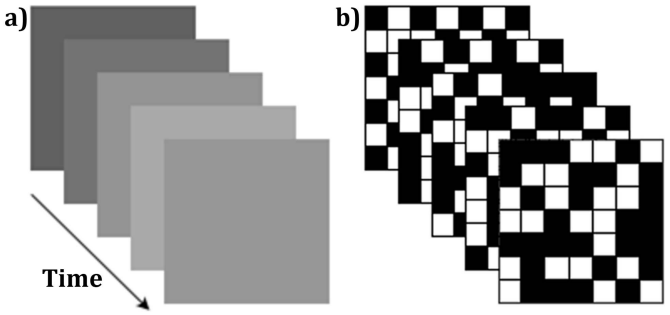

Fig. 6. Pseudorandom sequences. (a) Gaussian temporal sequence. (b) Spatiotemporal sequence.

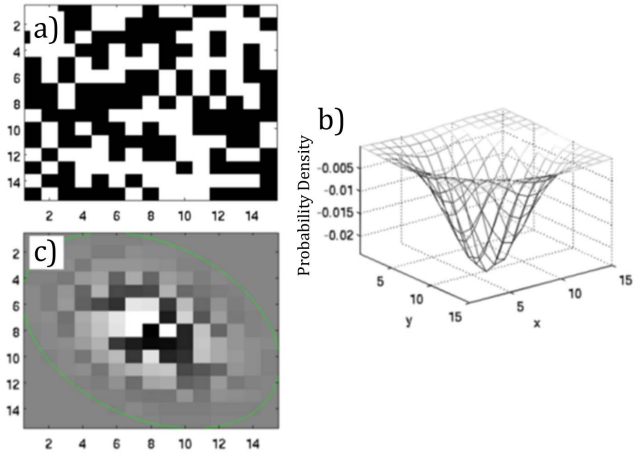

Fig. 7. Preprocessing step which shows how the local stimulus pertaining to a cell RF is weighted with a 2-D Gaussian filter. (a) Local stimulus for a cells RF. (b) 2-D Gaussian used to weight the stimulus intensities. (c) Weighted image of the local stimulus intensities.

is drawn again from a random sequence generated using the gasdev() function with an assigned value of either -0.5 or 0.5, independent of neighboring checkers. CBF is commonly used to determine characteristics of a cell's RF [42] and in this case, as a preprocessing step, it is cropped to the determined size of the RF region as shown in Fig. 7(c).

B. Data Preprocessing

The overall goal of the preprocessing stage is to manipulate the data so that they form a regression or classification data set, i.e., input–output corresponding to the stimulus–response, which then can be used for developing the computational models. Recordings were supplied for a number of ganglion cells and organized within two data sets, both containing the visual stimuli and neural spike responses. The first data set contained a large set of nonrepeated stimuli (2 16 000 samples for FFF and 2 58 000 samples for CBF) that are suitable to ascertain characteristics such as the STA and to ensure that a sufficient number of varied stimuli are presented in order to evoke cell responses. The second data set contained a much smaller set of stimuli (1200 samples), which were presented to the cells repeatedly.

Traditionally, only stimulus values within a cell's RF are considered for analysis as only values within this sensory

space contribute to a cell's response. However, as FFF stimulus has uniform spatial intensity throughout, there is no need to extract the specific stimulus in the region of the RGCs RF; thus, the average intensity of each presented image is extracted instead. The neural response, originally recorded as a frequency of 10 kHz, was binned at 30 Hz to align well with the stimulus input forming a single input–output data set.

As a preprocessing step for the CBF stimuli, the pertinent stimulus values must first be extracted from the checkerboard pattern [Fig. 7(a)]; here, we extract only those checkerboard values located either inside, or on the border of the cell's RF. The RF is determined using a standard reverse-correlation method [5], [14], which is a technique for studying how sensory neurons summate signals from different times and locations to generate a response [43].

To emulate the processing that occurs between the photoreceptors and RGCs, the local stimulus within the RF is weighted using a 2-D Gaussian filter (with a support of 3σ) [9], which is shown in Fig. 7(b). From the resulting weighted stimulus, shown in Fig. 7(c), the pixels within the region of the RF (green ellipse) are extracted and summed to form an input for the derived models. This results in a single value representing the CBF pattern for each time step rather than the individual pixel values (This is the standard approach [44] but, as it will be discussed later, the authors believe it merits further investigation into the use of 2-D inputs). The binned neural response is again used as the output which is binned according to the stimulus update rate. In the case of the second data set, i.e., the repeated trials, the mean of the binned spike rate is computed using the 43 trials and used as the model output.

IV. Result

Recordings of the ganglion cell neural responses (spikes) to the FFF and CBF stimulation were provided for a number of different ganglion cells. Here, we demonstrate the analysis of two selected ganglion cells for each stimulus set, one *ON-cell* and one *OFF-cell*. The cell type is traditionally characterized by the shape of its temporal profile (STA) [14], [45], [46], whilst the length of the temporal window can be assessed by examining the duration of the average response and ascertaining the point at which it converges to zero [14]. Fig. 8 shows the calculated profiles for both cells, where it was determined that 21 lagged values (700 ms) of the time series were sufficient to capture the required behavior. Fig. 8(a) shows a temporal profile akin to what is described as a biphasic OFF type cell in [45]; we refer to this cell simply as an *OFF-cell* in this paper. Fig. 8(b) shows a profile that is typical of an *ON-cell.*

A. Temporal Artificial Stimuli

Determining the STA profile of the cell is also useful for indicating the number of lagged values to use for training the models. For instance, for results presented in this section, it was estimated that 21 lagged values would be sufficient to train each algorithm. Upon further investigation, it was established that the use of ten lagged values, essentially capturing the main STA characteristics (Fig. 8(a) and (b)), was

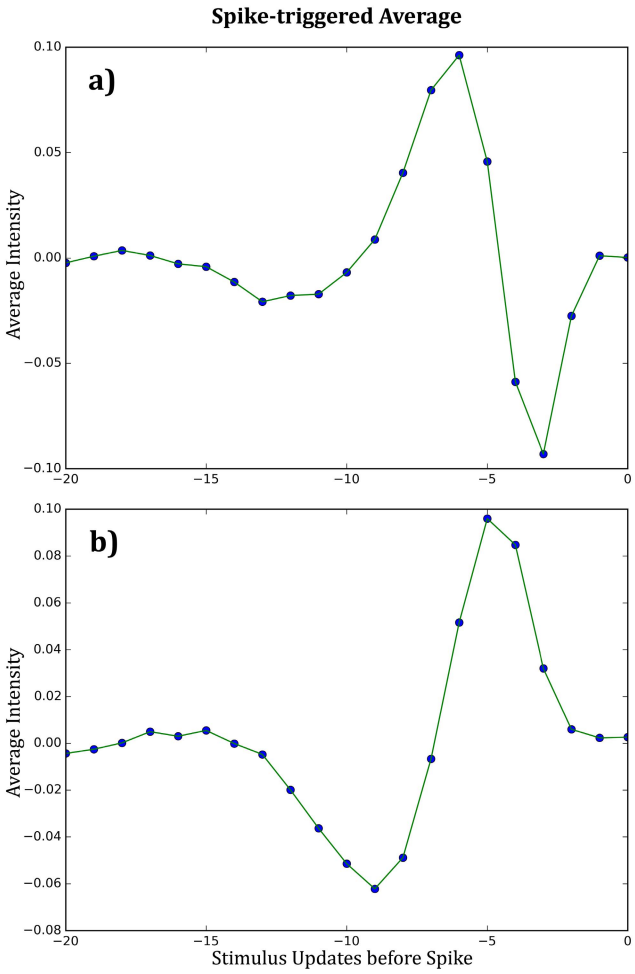

Fig. 8. STA profile of (a) *OFF-cell* and (b) *ON-cell* using FFF stimuli.

TABLE I
RMSE Values for OFF-Cell Using FFF Stimuli

Model	Training RMSE	Testing RMSE
LN	0.71	0.63
NARMAX	0.67	0.61
NARX	**0.52**	**0.49**
SOFNN	0.77	0.68

sufficient to train both the NARX and NARMAX methods and provided a marginal improvement in the estimated response. For the SOFNN method, however, the full range of STA values worked best.

Results of the derived models for the FFF stimuli are presented in Tables I and II, respectively. For each of the different approaches, model accuracy is measured using the root mean square error (RMSE) between the predicted and actual spike rate. From the results shown, it can be observed that the NARX method performs significantly better than the other investigated methods for both cells. Specifically, the performance increase of the NARX method over the

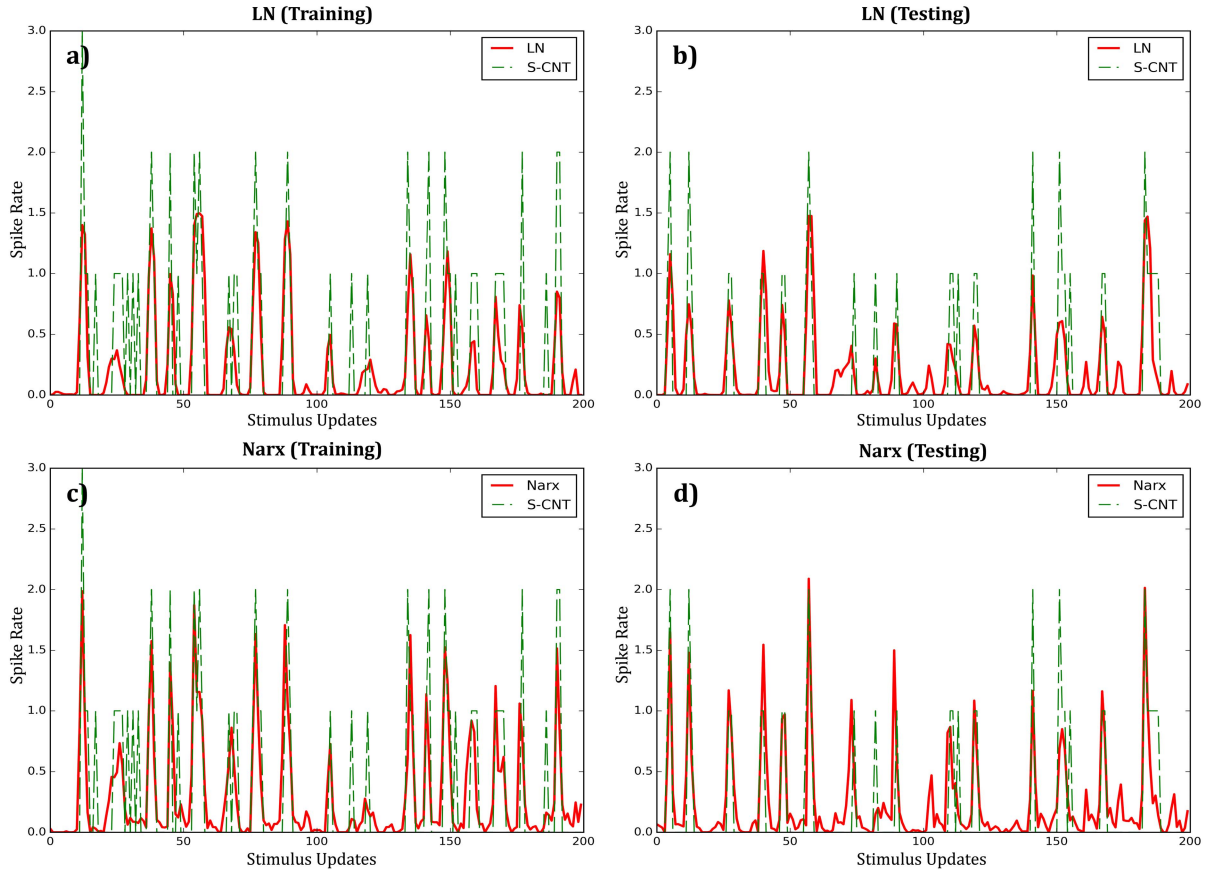

Fig. 9. Prediction results of the *ON-cell* model using the LN and NARX models for FFF stimuli for (a) training samples of the LN method, (b) testing samples of the LN method, (c) training samples of the NARX method, and (d) testing samples of the NARX method.

TABLE II
RMSE VALUES FOR ON-CELL USING FFF STIMULI

Model	Training RMSE	Testing RMSE
LN	0.37	0.35
NARMAX	0.38	0.37
NARX	**0.34**	**0.33**
SOFNN	0.42	0.41

LN method is quite substantial, with respect to the *OFF-cell* for both training and testing data sets. Surprisingly, integrating the previous errors of the system as controlled variables did not improve the predictive qualities of the model (Section II-C), as is evident by the NARMAX output.

Although the NARMAX approach achieved good results for the *OFF-cell* surpassing both the LN and SOFNN methods in performance, it did not improve upon the NARX model output which is less complex and requires considerably less computational power. Additionally, the SOFNN method, which has shown good performance in modeling output responses of isolated mice retinas [18], fails to provide an improved performance over the LN model for the salamander data.

To demonstrate the visible difference in performance of the NARX versus LN method, the training and testing outputs are shown in Fig. 9 for 200 samples. The results presented here are for the *ON-cell,* which shows the performance of the NARX method to be improved in terms of the magnitude even though performance in terms of RMSE is not as significant in comparison to the *OFF-cell*. This is evident when comparing Fig. 9(b) and (d), which relates to the testing output. It can be observed that both methods perform well in terms of predicting the timing of the spike rate though the NARX method additionally improves the magnitude of the predictions and in the majority of cases, reaches the target spike rate.

B. Spatiotemporal Artificial Stimuli

To increase the complexity of the derived models, such that they can generalize over a more complex stimulus set, the CBF data set is utilized. The results of the experiments for both data sets for the *OFF-cell* and *ON-cell* are outlined in Tables III and IV, respectively where model accuracy is measured in terms of the RMSE between the predicted and actual spike rate. Although the same cells are in use for these experiments, the stimulus sets differ and thus the results between data sets are not directly comparable. One observation, immediately noted, is that there is no clear separation between the performances of the LN approach versus the other investigated methods. This is discussed later.

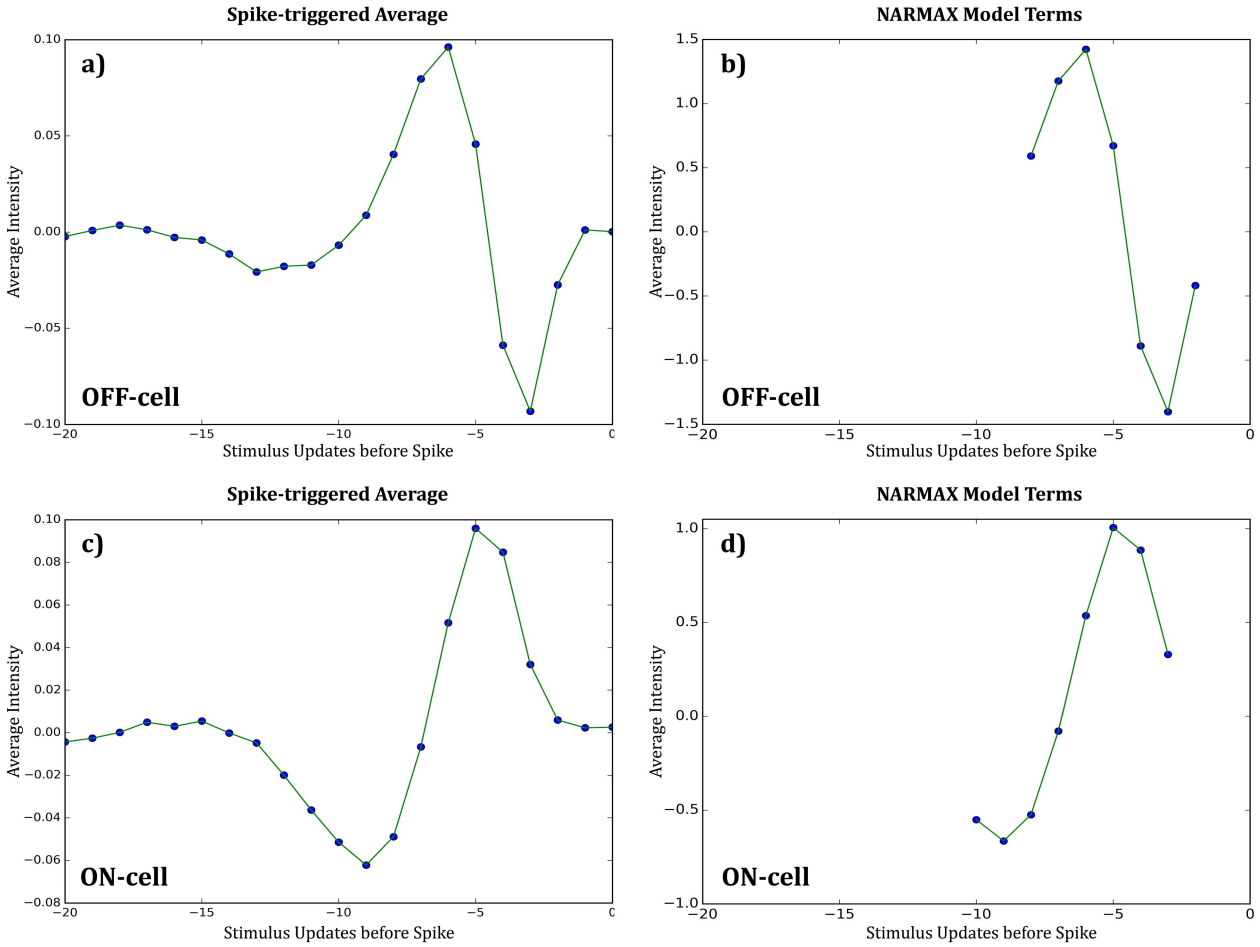

Fig. 10. Plot illustrating STA and linear terms from cubic NARMAX model showing (a) STA of the *OFF-cell*, (b) NARMAX terms for the *OFF-cell* model, (c) STA of the *ON-cell*, and (d) NARMAX terms for the *ON-cell* model.

TABLE III
RMSE VALUES FOR MODELS OF OFF-CELL USING CBF STIMULI

Model	Training RMSE (Dataset 1)	Testing RMSE (Dataset 1)	Testing RMSE (Dataset 2)
LN	0.35	**0.35**	**0.27**
NARMAX	0.35	0.36	0.28
NARX	**0.34**	**0.35**	**0.27**
SOFNN	0.36	0.37	0.30

TABLE IV
RMSE VALUES FOR MODELS OF ON-CELL USING CBF STIMULI

Model	Training RMSE (Dataset 1)	Testing RMSE (Dataset 1)	Testing RMSE (Dataset 2)
LN	0.38	0.38	**0.24**
NARMAX	0.39	0.38	0.25
NARX	**0.37**	**0.37**	**0.24**
SOFNN	0.39	0.38	0.27

In terms of the RMSE values, the NARX method outperforms the other models for both cells during the training phase. Within the testing data sets, however, the LN method performs on par with the NARX method for both testing sets with respect to the *ON-cell* and for the second data set with respect to the *OFF-cell*. Among the remaining system identification models, the NARMAX model outperforms the SOFNN model for both the *OFF-cell* and *ON-cell*, with the exception of the SOFNN model achieving an equivalent performance on 'Dataset 1' for the *ON-cell*. Emphasis is drawn to the fact that amongst the number of methods investigated, there is no significant improvement over the standard LN approach. We believe that, due to the increased spatial complexity of the stimulus, important information is being lost through the interpretation of the RF. This is currently achieved by extracting pertinent values inside the RF and simply summing or averaging to a single representative value. Interpreting the RF in this way disregards any spatial characteristics that

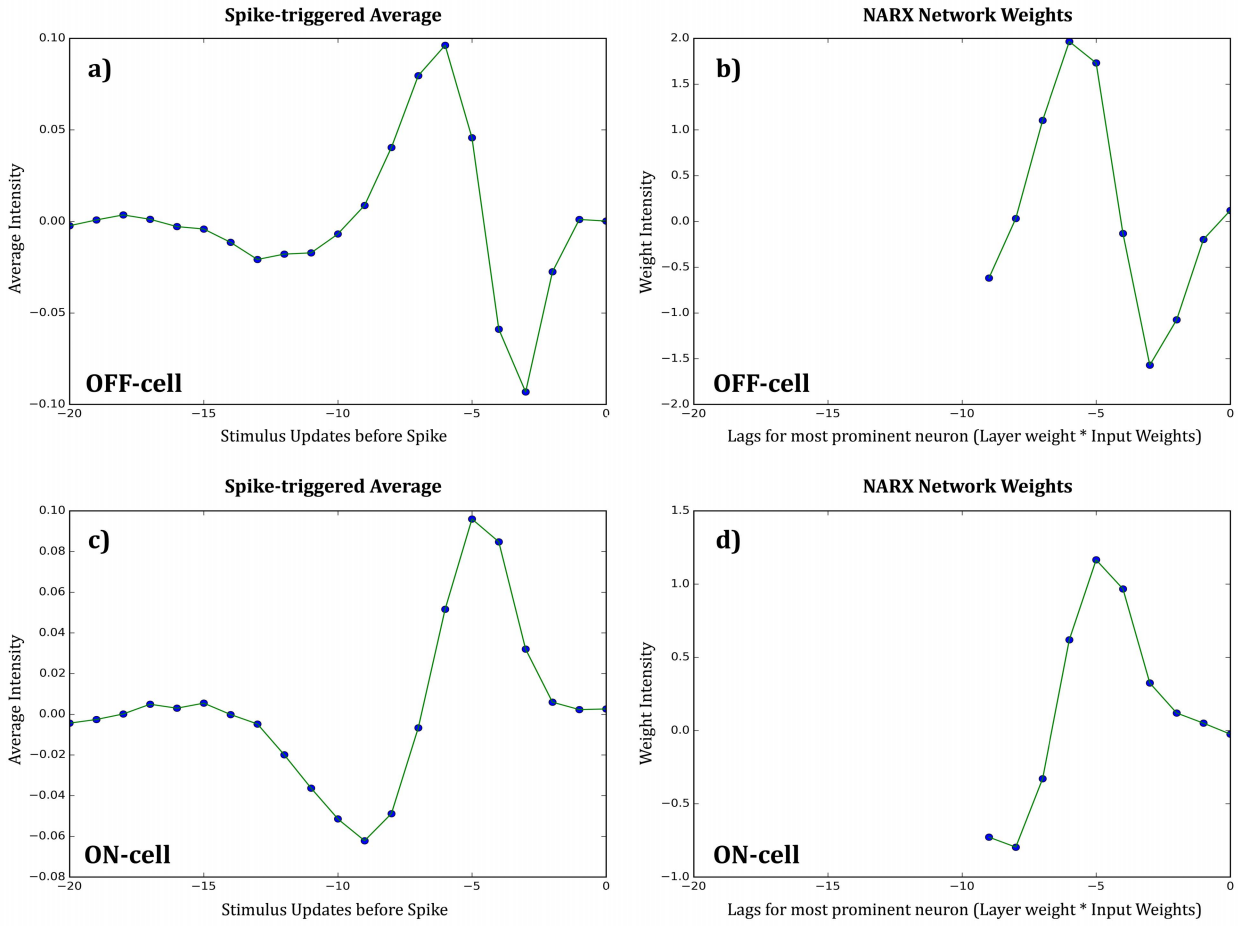

Fig. 11. Plot illustrating (a) STA of the *OFF-cell*, (b) NARX network weights for the *OFF-cell* model, (c) STA of the *ON-cell,* and (d) NARX network weights for the *ON-cell* model.

may have proven to be important to the cells behavior. This concept is explored further in Section V.

C. Model Analysis

The various models derived were analyzed further to ascertain any underlying system dynamics that may be of interest to provide areas for further investigation. Models developed for both the FFF and CBF stimulus showed similar characteristics when under review thus here we report only on the analysis for the FFF stimulus set.

Analysis of the NARMAX model reveals some interesting observations within the model terms. To discuss further, we first compute the STA using the standard approach reported in [14]. The terms for each derived NARMAX model are then plotted and compared to the STA. Fig. 10 illustrates the calculated STA and plotted NARMAX terms for both cells where the similarities between them are clearly observable. It is important to note that the NARMAX terms are based on what the model deems as important when it is being derived. Therefore, for the *OFF-cell*, Fig. 10(b) shows the terms considered most important when training the model, which suggest that dramatic changes in the stimulus contrast levels are important. This is also the case when comparing the STA and terms for the *ON-cell* which are shown in Fig. 10(c) and (d).

Due to the opaque nature of the NARX approach it is difficult to gain insight into any RGC models created using them. However, when analyzing the weights of the input and hidden layers, a similarity can also be drawn with the calculated STA of the cell. Fig. 11(a) and (b) shows this strong similarity when considering the most prominent neuron for the *OFF-cell*. Again, this is evident for the *ON-cell* shown in Fig. 11(c) and (d).

Finally, the SOFNN technique allows us to gain some insight into the underlying dynamics of the data by analyzing the fuzzy rules generated. An example of a rule generated by the SOFNN for the *OFF-cell* under FFF stimulation is shown in the Appendix. The result of plotting the coefficients of the consequent part of the rule is shown in Fig. 12(b). Remarkably, this approximately resembles the STA of the *OFF-cell*, which is shown in Fig.12(a) for comparison. This, therefore, shows that the response of the *OFF-cell* is due to a stark change in light intensity from high to low in comparison to the mean intensity level. Analyzing the rules for the *ON-cell* yields a similar outcome [Fig.12(c) and (d)].

The rules of the SOFNN are able to accurately portray how the model represents the input–output relationship, including

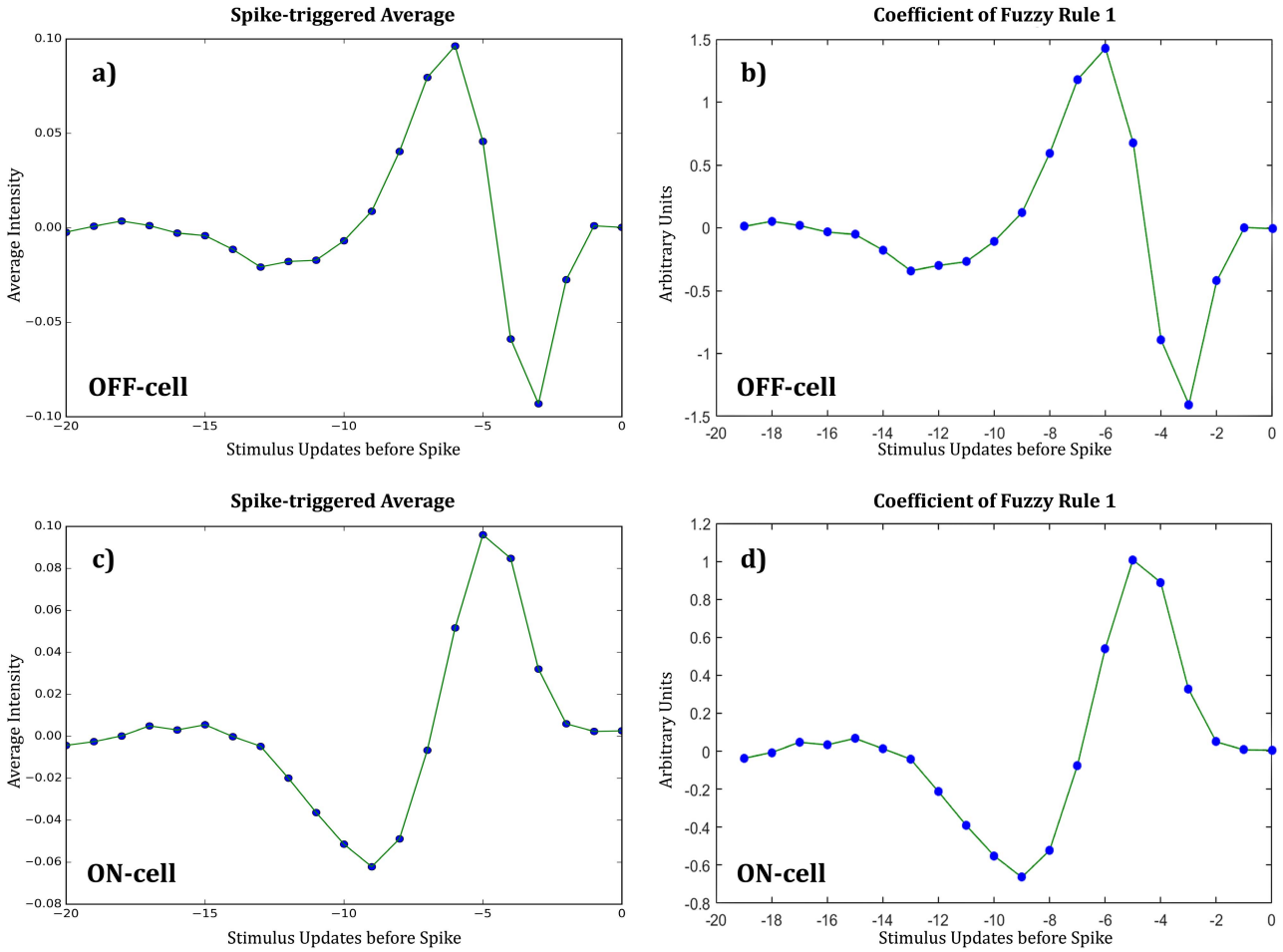

Fig. 12. Plot illustrating (a) STA of the *OFF-cell*, (b) coefficients of fuzzy rule for *OFF-cell* model, (c) STA of the *ON-cell,* and (d) coefficients of fuzzy rule for *ON-cell* model.

how input terms are combined and weighted to achieve the desired spike rate. This procedure is analogous to performing spike triggered analysis of the cell. In the case here, we have used artificial stimuli which means that it is difficult to gain an understanding if there is some spatial or temporal relationship of the inputs. However, the transparent nature of the model allows us to see what terms could be important if using targeted stimuli. We foresee that further experiments using targeted stimuli could help reveal the spatial and temporal relationship between the inputs which can help us gain an understanding of the underlying biological processes. This work is ongoing.

Both cells were adequately modeled by one neuron, corresponding to 1 fuzzy rule. Under CBF stimulation, the SOFNN model consisted of two neurons and consequently two fuzzy rules to model each cell. The increased network size, i.e., number of neurons, indicates that CBF stimuli are more complex to model than the FFF stimuli.

V. Discussion and Future Work

A. Discussion

Modeling RGCs within the retina is difficult due to insufficient knowledge about the internal components, their organization and the complexity of the interactions within the system. Existing computational models are traditionally derived by quantitatively fitting particular sets of physiological data using an input–output analysis involving computational combinations of linear and nonlinear models that are generally complex and lack any relevance to the underlying biophysics. The work outlined in this paper explores the application and feasibility of modeling RGCs with system identification techniques as an alternative to the traditional LN approach. We present results based on the application of a selection of system identification techniques, namely NARX, NARMAX, and SOFNN, to both temporal and spatiotemporal data revealing any underlying system dynamics that are observed after the modeling process. Although a performance increase is observable whilst stimulating the models with the FFF data set, the LN method still remains the best method when considering the spatiotemporal data.

The full-field temporal stimulus presented in Section III-A was the least complex stimulus considered for the work and consequently the explored models showed good performance in predicting the relationship between stimulus and response. In particular, the NARX method outperformed the other techniques in modeling both the *OFF-cell* and *ON-cell*. This performance increase is also clearly observable when reviewing

the model for the *ON-cell* which shows the least difference in terms of the RMSE when compared to the LN model. Surprisingly, the NARMAX method did not offer a better performance with its increased complexity through integration of previous errors as controlled variables. Although the results show that the NARMAX outperformed both the SOFNN and LN techniques, it was not able to outperform NARX which is significantly less complicated. The SOFNN did not perform as favourably in modeling the salamander RGCs but has shown good performance in past applications with mouse RGCs [18]. Its ability to capture characteristics that align well with the RGCs STA surpasses the representation observed through the NARMAX polynomial terms or the NARX internal layer weights though for this application it seems more appropriate to choose the simpler models that can generalise well over the input data, such as the NARX model.

With these interesting results for the temporal stimulus, we extended these modeling approaches to a more complex spatiotemporal stimulus (outlined in Section III-A). The spatiotemporal artificial stimuli increased the complexity of the stimulus as it introduced the need to process the RF information pertaining to each cell by extracting pixels within the region of interest, weighting with a Gaussian filter and summing the result. Of the methods investigated to model the relationship of the increased complexity between the input and output, the NARX method again performed favourably in comparison to the other methods investigated. However, where the NARX clearly performed better for the FFF data set, the difference observed between the NARX and LN within the CBF data set was diminished in terms of the RMSE. Here, the NARX had an improved performance with respect to the training data set for both cells but performed on par with the LN method for the testing sets. The NARMAX method provided a slightly improved performance over the SOFNN method for the *OFF-cell* but an equal performance for the *ON-cell*. Similarly, with the temporal data, characteristics akin to the STA of each cell were observable in all the system identification methods presented for the CBF data. The readability of such characteristics offers an advantage over more opaque approaches like LN that may provide a more in depth understanding of the underlying dynamics of the system, however further investigation into the relationship between these characteristics and the STA is ongoing.

Although the models presented adequately fit the real neural response, specifically the NARX method, there is quite a significant difference between the results for the temporal and spatiotemporal data sets. While not directly comparable, it can be observed that within the temporal data results, there is a clear separation between the performances of the standard LN approach versus the more bioinspired techniques. Analysis of the spatiotemporal results revealed results which were not as clearly discriminable and as such, the LN still remains the best model under the conditions tested.

Stemming from the comparative analysis between the temporal and spatiotemporal modeling approaches, we further investigated various aspects of the spatiotemporal modeling process. In particular, we questioned the transformation process of the RF and queried whether summing all of the spatial information to a singular representative value is sufficient enough to model an RGC efficiently. Given the increased complexity of the spatiotemporal data set compared with that of the temporal data set, it was hypothesised that summing the Gaussian weighted data within each RF was resulting in the significant loss of spatial information which could account for the increased complexity of fitting a model to the neural response. We also hypothesise that the loss of information explains the ability of the LN method to match or closely match the performance of newer, more sophisticated system identification techniques.

In [47], a method for retaining the spatial information is presented which calculates the STA spatially as well as temporally, filtering the stimulus with spatial information to create the input stimulus to a model. In this method, it is the LN method which benefits from this approach thus our initial investigation led to constructing the linear filter within the LN approach from spatial STA analysis. The results obtained from this approach were marginally better in terms of RMSE and the magnitude of the nonlinear estimate; however the associated computational cost would be extremely large for the NARX and other bioinspired methods without reducing the input space.

B. Future Work

Given the results outlined in this paper, further investigation is warranted into how the data within the RF is interpreted when dealing with stimuli containing a spatial component. The current method of collating all pixel information with the RF region ignores spatial information and as a result, models using CBF data perform on par with the standard LN method. To improve upon this result, additional inputs to the model would need to be considered which account for spatial variance in addition to temporal variance. However, to consider all pixel intensities would result in an increased computational cost thus there is a tradeoff between efficiency and model complexity to consider. Our future work will focus on different methods of compressing this information so that its influence is calculated correctly and with efficient computational complexity.

APPENDIX

An example rule generated by the SOFNN for the *OFF-cell* under FFF stimulation is as follows.

Rule 1: If Input 1 is A(−0.19113, 1.0375) AND Input 2 is A(0.15069, 1.0375) AND Input 3 is A(0.10993, 1.0375) AND Input 4 is A(−0.088315, 1.0375) AND Input 5 is A(0.30136, 1.0375) AND Input 6 is A(−0.085507, 1.0375) AND Input 7 is A(−0.064816, 1.0375) AND Input 8 is A(−0.08625, 1.0375) AND Input 9 is A(0.23699, 1.0375) AND Input 10 is A(−0.12157, 1.0375) AND Input 11 is A(−0.71477, 0.96985) AND Input 12 is A(0.15307, 1.0375) AND Input 13 is A(0.15517, 1.0375) AND Input 14 is A(0.16102, 1.0375) AND Input 15 is A(0.16543, 1.0375) AND Input 16 is A(−0.010237, 1.0375) AND Input 17 is A(0.074938, 1.0375) AND Input 18 is A(0.1176, 1.0375) AND Input 19 is A(0.00056977, 1.0375) AND Input 20 is A(−0.20507, 1.0375) THEN

Output: $0.33452 + -0.0070681 * \text{Input } 1 + 0.0029931 * \text{Input } 2 + -0.42334 * \text{Input } 3 + -1.4056 * \text{Input } 4 + -0.89218 * \text{Input } 5 + 0.67233 * \text{Input } 6 + 1.428 * \text{Input } 7 + 1.1801 * \text{Input } 8 + 0.59511 * \text{Input } 9 + 0.12145 * \text{Input } 10 + -0.10781 * \text{Input } 11 + -0.26965 * \text{Input } 12 + -0.29999 * \text{Input } 13 + -0.34188 * \text{Input } 14 + -0.17775 * \text{Input } 15 + -0.053445 * \text{Input } 16 + -0.034553 * \text{Input } 17 + 0.018151 * \text{Input } 18 + 0.050873 * \text{Input } 19 + 0.01101 * \text{Input } 20.$

Here, A (center, width) describes the membership function for each input. Similar to the machine learning models, the inputs to the SOFNN are lagged values of the stimulus sequence, so Input 1 corresponds to the current value of the series (i.e., 0-ms delay), and Input 20 corresponds to the value 19 time steps in the past (i.e., 700-ms delay).

ACKNOWLEDGMENT

The experimental data contributing to this paper have been supplied by the "Sensory Processing in the Retina" Research Group, Department of Ophthalmology, University of Göttingen as part of the VISUALISE Project.

REFERENCES

[1] C. I. Baker, "Behavioral neuroscience," in *Handbook of Psychology*, vol. 3, I. B. Weiner, R. J. Nelson, and S. Mizumori, Eds., 2nd ed. New York, NY, USA: Wiley, 2012.

[2] D. H. Hubel, *Eye, Brain, and Vision*, vol. 22. New York, NY, USA: Scientific American Library, 1988.

[3] J. L. Gauthier *et al.*, "Receptive fields in primate retina are coordinated to sample visual space more uniformly," *PLoS Biol.*, vol. 7, no. 4, p. e1000063, Apr. 2009.

[4] T. Gollisch and M. Meister, "Eye smarter than scientists believed: Neural computations in circuits of the retina," *Neuron*, vol. 65, no. 2, pp. 150–164, Jan. 2010.

[5] T. Gollisch and M. Meister, "Rapid neural coding in the retina with relative spike latencies," *Science*, vol. 319, no. 5866, pp. 1108–1111, Feb. 2008.

[6] W. F. Heine and C. L. Passaglia, "Spatial receptive field properties of rat retinal ganglion cells," *Vis. Neurosci.*, vol. 28, no. 5, pp. 403–417, Sep. 2011.

[7] J. W. Pillow *et al.*, "Spatio-temporal correlations and visual signalling in a complete neuronal population," *Nature*, vol. 454, no. 7207, pp. 995–999, Aug. 2008.

[8] B. P. Olveczky, S. A. Baccus, and M. Meister, "Segregation of object and background motion in the retina," *Nature*, vol. 423, no. 6938, pp. 401–408, May 2003.

[9] D. Kerr, T. M. McGinnity, S. Coleman, and M. Clogenson, "A biologically inspired spiking model of visual processing for image feature detection," *Neuro Comput.*, vol. 158, pp. 268–280, Jun. 2015.

[10] S. Shah and M. D. Levine, "Visual information processing in primate cone pathways. I. A model," *IEEE Trans. Syst., Man, Cybern. B, Cybern.*, vol. 26, no. 2, pp. 259–274, Apr. 1996.

[11] S. Ostojic and N. Brunel, "From spiking neuron models to linear-nonlinear models," *PLoS Comput. Biol*, vol. 7, no. 1, p. e1001056, Jan. 2011.

[12] J. W. Pillow, L. Paninski, V. J. Uzzell, E. P. Simoncelli, and E. J. Chichilnisky, "Prediction and decoding of retinal ganglion cell responses with a probabilistic spiking model," *J. Neurosci.*, vol. 25, no. 47, pp. 11003–11013, Nov. 2005.

[13] E. De Boer and P. Kuyper, "Triggered correlation," *IEEE Trans. Biomed. Eng.*, vol. BME-15, no. 3, pp. 169–179, Jul. 1968.

[14] E. J. Chichilnisky, "A simple white noise analysis of neuronal light responses," *Netw. Comput. Neural Syst.*, vol. 12, no. 2, pp. 199–213, Jan. 2001.

[15] C. Kayser, K. P. Kording, and P. Konig, "Processing of complex stimuli and natural scenes in the visual cortex," *Current Opinion Neurobiol.*, vol. 14, no. 4, pp. 468–473, Aug. 2004.

[16] D. J. Livingstone, *Artificial Neural Networks: Methods and Applications Methods in Molecular Biology*. Totowa, USA: Humana Press, 2008.

[17] N. P. P. A. Sousa, "Neural encoding models in natural vision," Ph.D. dissertation, Eng. Faculty Univ. Porto, Porto, Portugal, 2013.

[18] S. McDonald, D. Kerr, S. Coleman, P. Vance, and T. M. McGinnity, "Modelling retinal ganglion cells using self-organising fuzzy neural networks," in *Proc. Int. Joint Conf. Neural Netw. (IJCNN)*, Jul. 2015, pp. 1–8.

[19] D. Kerr, S. Coleman, and T. McGinnity, "Modelling and analysis of retinal ganglion cells with neural networks," in *Proc. Irish Mach. Vis. Image Process.*, Sep. 2014, pp. 95–100.

[20] G. P. Das, P. Vance, D. Kerr, S. A. Coleman, and T. M. McGinnity, "Modelling retinal ganglion cells stimulated with static natural images," in *Proc. Int. Conf. Adv. Cognit. Technol. Appl.*, 2016, p. 6.

[21] S. A. Billings and W. S. F. Voon, "Least squares parameter estimation algorithms for non-linear systems," *Int. J. Syst. Sci.*, vol. 15, no. 6, pp. 601–615, Apr. 1984.

[22] U. Friederich, D. Coca, S. Billings, and M. Juusola, "Data modelling for analysis of adaptive changes in fly photoreceptors," in *Proc. Int. Conf. Neural Inf. Process.*, 2009, pp. 34–48.

[23] D. Kerr, U. Nehmzow, and S. Billings, *Towards Automated Code Generation for Autonomous Mobile Robots*. Paris, France: Atlantis Press, 2010.

[24] Y. Gao and M. J. Er, "NARMAX time series model prediction: Feedforward and recurrent fuzzy neural network approaches," *Fuzzy Sets Syst.*, vol. 150, no. 2, pp. 331–350, Mar. 2005.

[25] S. A. Billings, *Nonlinear System Identification: NARMAX Methods in the Time, Frequency, and Spatio-Temporal Domains*. Hoboken, NJ, USA: Wiley, 2013.

[26] D. Kerr, M. McGinnity, and S. Coleman, "Modelling and analysis of retinal ganglion cells through system identification," in *Proc. Int. Conf. Neural Comput. Theory Appl.* 2014, pp. 158–164.

[27] P.-F. Alvanitopoulos *et al.*, "Solar radiation time-series prediction based on empirical mode decomposition and artificial neural networks," in *Proc. 10th IFIP WG Int. Conf., Artif. Intell. Appl. Innov. (AIAI)*, vol. 436. Rhodes, Greece, Sep. 2014, pp. 467–475.

[28] H. T. Siegelmann, B. G. Horne, and C. L. Giles, "Computational capabilities of recurrent NARX neural networks," *IEEE Trans. Syst., Man, Cybern. B, Cybern.*, vol. 27, no. 2, pp. 208–215, Apr. 1997.

[29] M. Bianchini, M. Maggini, and L. C. Jain, *Handbook on Neural Information Processing*. Berlin, Germany: Springer, 2013.

[30] E. Petrovic, Z. Cojbasic, D. Ristic-Durrant, V. Nikolic, I. Ciric, and S. Matic, "Kalman Filter and NARX neural network for robot vision based human tracking," *Facta Universitat., Ser. Autom. Control Robot.*, vol. 12, no. 1, pp. 43–51, Jul. 2013.

[31] H. Xie, H. Tang, and Y.-H. Liao, "Time series prediction based on NARX neural networks: An advanced approach," in *Proc. Int. Conf. Mach. Learn. Cybern.*, Jul. 2009, pp. 1275–1279.

[32] A. Hornstein and U. Parlitz, "Bias reduction for time series models based on support vector regression," *Int. J. Bifurcation Chaos*, vol. 14, no. 06, pp. 1947–1956, Jun. 2004.

[33] S. A. Billings and D. Coca, "Identification of NARMAX and related models," Dept. Autom. Control Syst. Eng., Encyclopedia Life Support Syst. (ELOSS), Res. Rep.-Univ. Sheffield, 2001.

[34] S. Chen and S. Billings, "Representations of non-linear systems: The NARMAX model," *Int. J. Control*, vol. 49, no. 3, pp. 1013–1032, Mar. 1989.

[35] G. Leng, G. Prasad, and T. A. McGinnity, "A new approach to generate a self-organizing fuzzy neural network model," in *Proc. IEEE Int. Conf. Syst., Man Cybern.*, Oct. 2002, p. 6.

[36] G. Leng, T. M. McGinnity, and G. Prasad, "Design for self-organizing fuzzy neural networks based on genetic algorithms," *IEEE Trans. Fuzzy Syst.*, vol. 14, no. 6, pp. 755–766, Dec. 2006.

[37] G. Leng, T. M. McGinnity, and G. Prasad, "An approach for on-line extraction of fuzzy rules using a self-organising fuzzy neural network," *Fuzzy Sets Syst.*, vol. 150, no. 2, pp. 211–243, Mar. 2005.

[38] G. Leng, G. Prasad, and T. M. McGinnity, "An on-line algorithm for creating self-organizing fuzzy neural networks," *Neural Netw.*, vol. 17, no. 10, pp. 1477–1493, Dec. 2004.

[39] T. Takagi and M. Sugeno, "Fuzzy identification of systems and its applications to modeling and control," *IEEE Trans. Syst., Man, Cybern. B, Cybern.*, vol. SMC-15, no. 1, pp. 116–132, Jan./Feb. 1985.

[40] J. K. Liu and T. Gollisch, "Spike-triggered covariance analysis reveals phenomenological diversity of contrast adaptation in the retina," *PLoS Comput. Biol.*, vol. 11, no. 7, p. e1004425, Jul. 2015.

[41] W. H. Press, *Numerical Recipes*, 3rd ed. Cambridge, U.K.: Cambridge Univ. Press, 2007.

[42] T. Gollisch and M. Meister, "Modeling convergent ON and OFF pathways in the early visual system," *Biol. Cybern.*, vol. 99, nos. 4–5, pp. 263–278, Nov. 2008.
[43] D. Ringach and R. Shapley, "Reverse correlation in neurophysiology," *Cognit. Sci.*, vol. 28, no. 2, pp. 147–166, Mar./Apr. 2004.
[44] G. W. Schwartz *et al.*, "The spatial structure of a nonlinear receptive field," *Nature Neurosci.*, vol. 15, no. 11, pp. 1572–1580, Nov. 2012.
[45] R. Segev, J. Puchalla, and M. J. Berry, "Functional organization of ganglion cells in the salamander retina," *J. Neurophysiol.*, vol. 95, no. 4, pp. 2277–2292, Apr. 2006.
[46] D. R. Cantrell, J. Cang, J. B. Troy, and X. Liu, "Non-centered spike-triggered covariance analysis reveals neurotrophin-3 as a developmental regulator of receptive field properties of ON-OFF retinal ganglion cells," *PLoS Comput. Biol.*, vol. 6, no. 10, p. e1000967, Oct. 2010.
[47] O. Schwartz, J. W. Pillow, N. C. Rust, and E. P. Simoncelli, "Spike-triggered neural characterization," *J. Vis.*, vol. 6, no. 4, p. 13, Feb. 2006.

Philip J. Vance received the B.Eng. degree (Hons.) in electronics and computing and the Ph.D. degree from Ulster University, Coleraine, U.K., in 2006 and 2011, respectively.

He was with the Digital Health Group, Intel, where he was involved in health-assisted applications. In 2011, he was employed in a consultancy-based embedded systems role with the EpiCentre, Londonderry U.K., where he was involved in developing and testing prototype embedded platforms. He was involved in numerous research projects, including IM-CLeVeR, RUBICON, VISUALISE, and SLANDAIL FP7 EU. He is currently within a research role within the Intelligent Systems Research Centre, Ulster University. He has authored or co-authored over 14 research papers and has been involved in the writing of many research grant proposals.

Dr.Vance was a recipient of the Asidua Prize for Embedded Systems.

Gautham P. Das received the B.Tech. degree (Hons.) in instrumentation and control engineering from the University of Calicut, Calicut, India, in 2003, the M.Tech. degree (Hons.) in electrical engineering from IIT Roorkee, Roorkee, India, in 2006, and the Ph.D. degree from Ulster University, Coleraine, U.K., in 2015.

He was a Research Associate with the School of Computing and Intelligent Systems, Ulster University. He is currently an Assistant Professor with the Department of Mechanical Engineering, Amrita Vishwa Vidyapeetham University, Coimbatore, India. His current research interests include computational modeling, intelligent systems, multirobot systems, and the application of artificial intelligence in robotics.

Dermot Kerr received the B.Sc. degree (Hons.) in computing science and the Ph.D. degree in computing and engineering from Ulster University, Coleraine, U.K., in 2005 and 2008, respectively.

He is currently a Lecturer with the School of Computing and Intelligent System, Ulster University. His current research interests include biologically inspired image processing, mathematical image processing, feature detection, omnidirectional vision, system identification, and robotics.

Dr. Kerr is an Officer and a member of the Irish Pattern Recognition and Classification Society. He is currently Co-Investigator on the EU FP7 funded project SLANDAIL and was Co-Investigator on the EU FP7 FET VISUALISE Project.

Sonya A. Coleman received the B.Sc. degree (Hons.) in mathematics, statistics, and computing and the Ph.D. degree in mathematics from Ulster University, Coleraine, U.K., in 1999 and 2003, respectively.

She was Co-I on EU FP7 projects VISUALISE and RUBICON. She is currently a Principle Investigator of the Capital Markets Engineering Studentship program, and a Co-I on the Capital Markets Collaborative Network Project and the EU FP7 SLANDAIL Project. She is also a Professor of Vision Systems with the School of Computing and Intelligent System, Ulster University, and also the Cognitive Robotics Team Leader with the Intelligent Systems Research Centre. She has authored or co-authored over 130 publications primarily in robotics, image processing, bioinspired systems, and computational finance.

Dr. Coleman was awarded the Distinguished Research Fellowship by Ulster University in recognition of her contribution to research. She received research funding from various sources such as EPSRC (EP/C006283/1), The Nuffield Foundation, The Leverhulme Trust, and the EU.

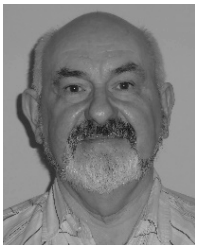

T. Martin McGinnity (SM'83) received the Degree (Hons.) in physics in 1975, and the Ph.D. degree in electronics from the University of Durham, Durham, U.K., in 1979.

He was a Professor of Intelligent Systems Engineering and the Director of the Intelligent Systems Research Centre, Faculty of Computing and Engineering, Ulster University, Coleraine, U.K. He is currently a Pro-Vice-Chancellor of student affairs and the Head of the College of Science and Technology, Nottingham Trent University, Nottingham, U.K. He has authored or co-authored over 300 research papers. He raised over £25 million in research funding. His current research interests include computational intelligence, computational neuroscience, modeling of biological information processing, and cognitive robotics.

Dr. McGinnity is a fellow of IET.

Tim Gollisch received the Degree (Hons.) in physics from the University of Heidelberg, Heidelberg, Germany, and the Ph.D. degree in biophysics from Humboldt University Berlin, Berlin, Germany.

He is currently a Professor of Sensory Processing in the Retina with the Ophthalmology Department, University Medical Center Göttingen, Göttingen, Germany. He has been involving on combining experimental and theoretical approaches to study sensory systems for more than a decade and has focused on the retina for the last few years. His research has been published in highly regarded scientific journals, including *Science* and *Neuron*.

Dr. Gollisch has received several personal research fellowships, such as Boehringer Ingelheim Fonds Fellowship, HFSP Long-Term Fellowship, and the HFSP Career Development Award.

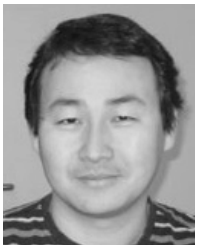

Jian K. Liu received the B.S. degree in theoretical mechanics from Jilin University, Changchun, China, in 2001, the M.S. degree in fluid mechanics from Peking University, Beijing, China, in 2004, and the Ph.D. degree in mathematics from UCLA, Los Angeles, CA, USA, in 2009.

He was with the Department of Ophthalmology, University Medical Center Göttingen, Göttingen, Germany, and also with the Bernstein Center for Computational Neuroscience Göttingen, Göttingen, Germany. He is currently an Assistant Professor with the Institute for Theoretical Computer Science, Graz University of Technology, Graz, Austria. His current research interests include computational neuroscience, brain-like computation, and the application of artificial intelligence in robotics.